SCIENCE AND INNOVATION
INTERNATIONAL SCIENTIFIC JOURNAL VOLUME 3 ISSUE 4 APRIL 2024
ISSN: 2181-3337 | SCIENTISTS.UZ

DIAGNOSIS OF EAR DISEASES USING A HYBRID NEURAL NETWORK

Sayyora Iskandarova[1], Nozima Atadjanova[2], Gulzira Khaldarova[3], Makhliyo Turaeva[4]
[1,2,3,4]Tashkent University of Information Technologies named after Muhammad Al-Khwarizmi
Department of Computer Systems, Tashkent
https://doi.org/10.5281/zenodo.10973392

Abstract. *This article, focuses on the diagnosis of diseases of the inner ear. Fuzzy image processing and its efficiency are covered in the problem of image classification. The dataset was created from the processed images. An analysis of the results obtained by the CNN-LSTM-ELM hybrid neural network is presented.*

Keywords*: image processing, fuzzy set, fuzzy, hybrid neural network.*

Introduction

Nowadays, thanks to the development of technologies and methods, it has become easier to predict medical problems. Due to the complexity of the technique and technology of neural networks, the level of their accuracy has increased. One of the most important tasks in diagnosis is to distinguish disease symptoms [1]. Cholesteatomas are benign collections of keratinized squamous epithelium mostly found within the middle ear; however, they are intractable chronic proliferative diseases that can cause fatal complications such as bone destruction and brain abscesses. Surgery is the only treatment option, and long-term relapses have been reported even with appropriate surgery. Various surgical procedures depend on the extent of the lesion, especially its extension to the mastoid process. This influences surgical approaches, including the choice of minimally invasive endoscopic surgery or behind-the-ear microsurgery. However, the present imaging examinations cannot adequately confirm the extent of the lesion, which may necessitate intraoperative modification of the approach and significantly prolong the operative time [2-4].

Image recognition image processing algorithm

Algorithms for extracting features.

Typically, the extraction of features in the image includes the following main steps:

1. Obtaining a normalized gray image;
2. Search for Region of Interest(RoI);
3. Isolation of the boundaries of the RoI (Sobel, Laplace, Kani, etc. methods);
4. Turning the area under consideration into a monochrome image;
5. Analysis of the obtained monochrome and gray images in the study area [5-6].

The following classical formula is used to obtain a grayscale image:

$I(C)=0,3\cdot R(C)+0,59\cdot G(C)+0,11\cdot B(C)$.

where I is the intensity at the gray point of the image, R, G and B (values 0.255) are the red, green and blue components of the color C.

Algorithm for Fuzzy Clustering of Sets of Real Numbers.

Let the set of real numbers $X=\{x_1,x_2,..,x_m\}\subset R$ and k real numbers $s_1,s_2,..,s_k$ be given in ascending order:

$$s_1<s_2,<..<s_k$$

Fuzzification $A_1, A_2, .., A_k$ for the set X can be done using the triangular function.

Let a≠b be two real numbers. An open triangular function can be defined as:

$$\mu(x,b;a) = \max\left[\min\left(1, \frac{x-a}{b-a}\right), 0\right]. \quad (1)$$

If a<b, (1) defines a right-open triangular function, and if a>b, formula (1) defines a left-open triangular function.

Note that μ checks for the following four properties:

$$\mu(a,b;a) = 0,$$
$$\mu(b,b;a) = 1,$$
$$\mu(\frac{a+b}{2}, b;a) = \frac{1}{2},$$
$$\mu(x,b;a) + \mu(x,a;b) = 1. \quad (2)$$

Expression (2) shows that the functions $\mu(x,b;a)$ and $\mu(x,a;b)$ determine the fuzzy domain of the space R.

Let a<b<c be three real numbers. The trigonometric function can be defined as:

$$t(x,b;a,c) = \mu(x,b;a) \wedge \mu(x,b;c), \quad (3)$$

where ∧ refers to the function "min" or algebraic multiplication "·".

In other words, a fuzzy set is defined by a triangular membership function, which is the intersection of two open fuzzy sets [8-9].

You can find other formulas for calculating the trigonometric function. This function will look like this: $\mu(x,b;a) = \alpha \cdot |x-a| + \beta|x-b| + \gamma|x-c|$.

The function parameters μ(a), μ (b), μ (c) are determined by the values of the functions at points a, b, c. To do this, you need to solve the following system of equations:

$$\begin{cases} \beta|a-b| + \gamma|a-c| = \mu(a,b;a) \\ \alpha|b-a| + \gamma|b-c| = \mu(b,b;a) \\ \alpha|c-a| + \beta|c-b| = \mu(c,b;a) \end{cases} \quad (4)$$

The system of equations (4) has the following solution:

$$\begin{cases} \alpha = \frac{1}{2} \cdot \left(\frac{\mu(c,b;a) + \mu(a,b;a)}{c-a} + \frac{\mu(b,b;a) - \mu(a,b;a)}{b-a} \right) \\ \beta = \frac{1}{2} \cdot \left(\frac{\mu(c,b;a) - \mu(b,b;a)}{c-b} + \frac{\mu(b,b;a) - \mu(a,b;a)}{b-a} \right). \\ \gamma = \frac{1}{2} \cdot \left(\frac{\mu(c,b;a) + \mu(a,b;a)}{c-a} - \frac{\mu(c,b;a) - \mu(b,b;a)}{c-b} \right) \end{cases}$$

For specific values of functions $\mu(a) = 0,\ \mu(b) = 1,\ \mu(c) = 0,$, the solution will look like this:

$$\begin{cases} \alpha = \frac{1}{2} \cdot \frac{1}{b-a} \\ \beta = \frac{1}{2} \cdot \left(\frac{1}{b-a} - \frac{1}{c-b} \right) \\ \gamma = \frac{1}{2} \cdot \frac{1}{c-b} \end{cases}$$

and

$$\mu(x,b;a) = \frac{1}{2} \cdot \frac{|x-a|}{b-a} + \frac{1}{2} \cdot \left(\frac{1}{b-a} - \frac{1}{c-b} \right) \cdot |x-b| + \frac{1}{2} \cdot \frac{|x-c|}{c-b}$$

or

$$\mu(x,b;a) = \frac{1}{2} \cdot \frac{|x-a| - |x-b|}{b-a} + \frac{1}{2} \cdot \frac{|x-c| - |x-b|}{c-b} \quad (5)$$

In the same way, we can get a similar formula for an open triangular function. Function for two real numbers a≠b:

$$\mu(x,b;a)=\frac{1}{2}\cdot\frac{|x-a|-|x-b|}{b-a}+\frac{1}{2} \qquad (6)$$

an open triangle defines a function. From a practical point of view, instead of formula (6), the following formula can be used:

$$\mu(x,b;a)=\frac{1}{2}\cdot\frac{|x-a|-|x-b|+\varepsilon}{|b-a|+\varepsilon}+\frac{1}{2} \qquad (7)$$

here

$$1>>\varepsilon>0 \quad (8)$$

More generally, we can say that $A_1, A_2, .., A_k$ is fuzzy for a set X using the L-R functions.

A fuzzy number $\tilde{x}$ is called a fuzzy number of type L - R if:

$$\mu(\mathrm{x}, \mathrm{x}_R(\alpha), \mathrm{x}_L(\alpha))=\begin{cases}\mu_L(x)=1-\dfrac{x-x_L(\alpha)}{u_L},\\ \mu_R(x)=1-\dfrac{x_R(\alpha)-x}{x_R},\end{cases} \qquad (8)$$

if here χ is the value of a fuzzy number, i.e. $x=x_L(1)=x_R(1)$; x_L and x_R are the left and right extensions of the fuzzy number $\tilde{x}$, respectively; $x_L(\alpha)$ and $x_R(\alpha)$ are the left and right values of the fuzzy number α of clarity $\tilde{u}$, respectively.

It follows from the definition that if $\tilde{x}(\alpha)=\{x, x_L(\alpha), x_R(\alpha)\}$ is equal, then $x_L(\alpha)=x-(1-\alpha)x_L$ $x_R(\alpha)=x+(1-\alpha)x_R$ is equal.

We consider the following type of algebraic operation on L-R fuzzy sets:

Addition:

$$\tilde{u}+\tilde{v}=\{u+v-(1-\alpha)(u_L+v_L);u+v+(1-\alpha)(u_R+v_R)\}$$

Subtraction:

$$\tilde{u}-\tilde{v}=\{u-v-(1-\alpha)(u_L+v_L);u-v+(1-\alpha)(u_R+v_R)\}$$

Multiplication:

1) for $u>0; v>0$

$$\tilde{u}\cdot\tilde{v}=\{u\cdot v;(1-\alpha)(uv_L+vu_L)-(1-\alpha)u_Lv_L;(1-\alpha)(uv_R+vu_R)+(1-\alpha)u_Rv_L\};$$

2) for $u>0; v<0$

$$\tilde{u}\cdot\tilde{v}=\{u\cdot v;(1-\alpha)(uv_R+vu_L)-(1-\alpha)u_Lv_L;(1-\alpha)(uv_L+vu_R)+(1-\alpha)u_Rv_L\};$$

3) for $u<0; v<0$

$$\tilde{u}\cdot\tilde{v}=\{u\cdot v;(1-\alpha)(uv_R+vu_L)-(1-\alpha)u_Rv_R;(1-\alpha)(uv_L+vu_L)-(1-\alpha)u_Lv_L\}.$$

Division:

$$\frac{\tilde{u}}{\tilde{v}}=\tilde{u}\cdot\frac{1}{\tilde{v}}$$

When developing a fuzzy clustering algorithm for image segmentation, we will first define the membership function:

$$\mu_1(x)=\mu(x,s_1;s_2)$$

i=2,3, ..., for k−1

$$\mu_i(x)=\mu(x,s_i;s_{i-1})\wedge\mu(x,s_i;s_{i+1})$$

$$\mu_k(x)=\mu(x,s_k;s_{k-1})$$

$\mu_1, \mu_2, .., \mu_k$ functions define a division section by the following equality:

$$\mu_1 + \mu_2 + ... + \mu_k = 1$$

Second, the defuzzification operator $\tau(\mu, \gamma)$ used for fuzzy segmentation is defined:

$$\tau(\mu, \gamma) = (\tau_1, \tau_2, .., \tau_k)$$

here,

$$\tau(x, \mu, \gamma) = \frac{\mu_i^{\gamma}(x)}{\sum_{j=1}^{k} \mu_i^{\gamma}(x)} \qquad (9)$$

Suppose v_1 and F_1 are defined as follows:

$$v_i(x) = \mu_i(x) \wedge \tau_i(x, \mu; \gamma), \qquad (10)$$

$$F_i(s_i) = \frac{\sum_{j=1}^{m} v_i(x_j) \cdot x_j}{\sum_{j=1}^{m} v_i(x_j)}. \qquad (11)$$

Now consider the following constraint on $s_1, s_2, .., s_k$ parameters:

$$s_i = F_i(s_i) \qquad (12)$$

The fuzzy set A_i is defined by equation (2.12). The center s_i belongs to the convex hull of the set X and is a fixed point for the function F_i.

The results are obtained using the following fuzzy clustering algorithm.

Step 1. The number of clusters is equal to k, the defuzzification parameter is γ, the process stop parameter is δ, the iteration index is l=0, the initial values are given to the cluster centers. Then $\mu_1^{(0)}, \mu_2^{(0)}, .., \mu_k^{(0)}$ are fuzzy membership functions and components of the defuzzification of $\tau_1^{(0)}, \tau_2^{(0)}, .., \tau_k^{(0)}$ functions.

Step 2. Increase the iteration index, that is, calculate $l \to l+1$. Cluster centers $s_1^{(l)} = F_1(s_1^{(l-1)}), s_2^{(l)} = F_2(s_2^{(l-1)}), ..., s_k^{(l)} = F_k(s_k^{(l-1)})$, $\mu_1^{(l)}, \mu_2^{(l)}, .., \mu_k^{(l)}$ fuzzy membership functions, $\tau_1^{(l)}, \tau_2^{(l)}, .., \tau_k^{(l)}$ defuzzification components, and $v_1^{(l)}, v_2^{(l)}, .., v_k^{(l)}$ functions.

Step 3. We calculate $d = \sum_{i=1}^{k} \left| \mu_i^{(l)} - \mu_i^{(l-1)} \right|$. If d>δ, go back to step 2, otherwise go to step 4.

Step 4. Save the data and you are done.

Thus, the images are subjected to digital processing and computer vision, and a data set is formed based on the processed images.

Image classification with hybrid neural network

CNN-LSTM-ELM is a hybrid neural network consisting of a combination of a convolution operation, an LSTM (Long Short-Term Memory) classifier, and an ELM (Extreme Learning Machine). The CNN-LSTM-ELM algorithm has been proposed for ear image recognition (HAR Human Activity Recognition). He used a database of 3495 training samples to evaluate the hybrid neural network architecture. This model was trained and tested using a GPU with 1536 cores, clocked at 1050 MHz and 8 GB of RAM. Figure 1 shows the general architecture of the CNN–LSTM–ELM model [10–11].

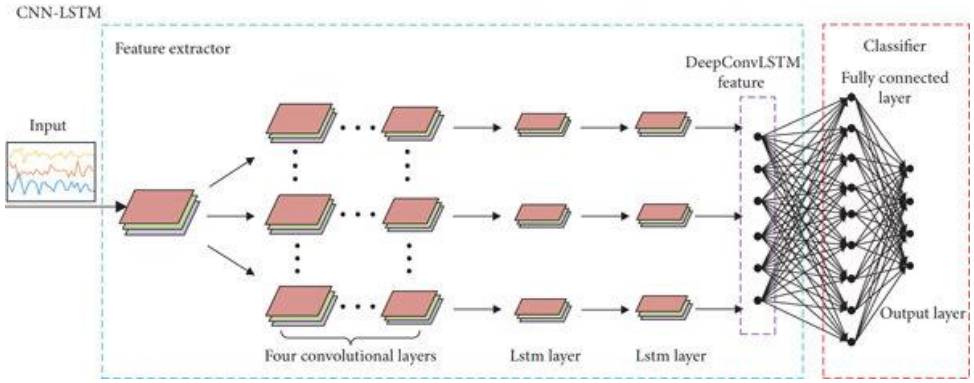

Fig. 1. CNN-LSTM-ELM model.

A graph of the accuracy of the model generated by training hybrid neural network models based on this Figure 1 was obtained by training selected images.

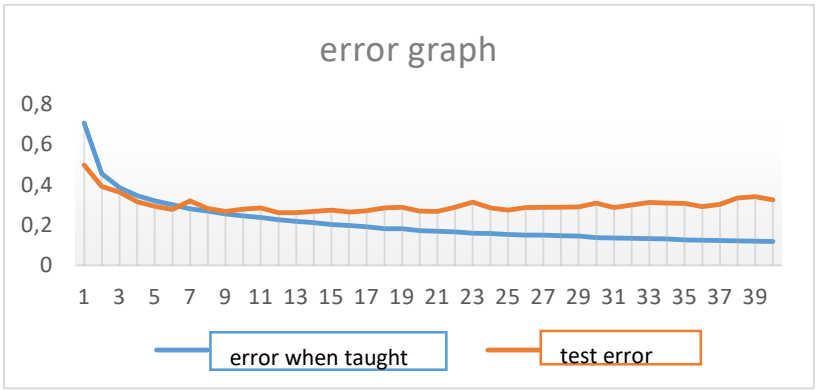

Fig. 2. Error graph of a model built on the basis of a convolutional neural network

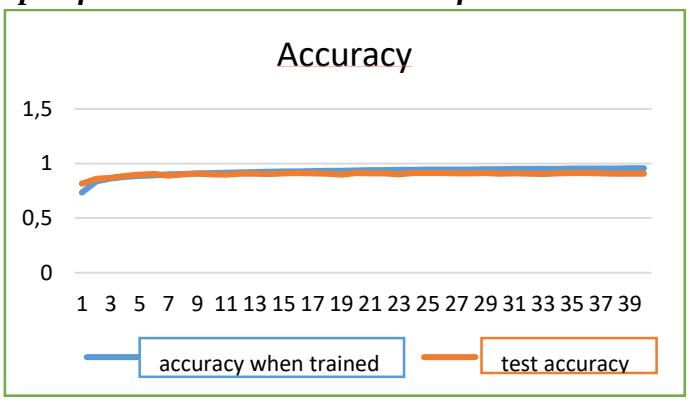

Fig. 3. Graph of the accuracy of the model built on the basis of a convolutional neural network.

Based on the method of training a hybrid neural network with a teacher, software was created for recognition and classification of objects, on the basis of which the results presented in Table 3 were obtained.

Table 1. Study samples used in the experiments.

№	Name of category	Total training
1	Cholesteatoma	1500
2	Healthy ear	1500

The optimal number of epochs (iterations) was determined by training, transforming and testing the selected network.

Table 2. When training on test data unfamiliar to the system.

№	Name of category	Total tests	Right	Incorrect	Percent
1	Cholesteatoma	45	214	31	87,6
2	Healthy ear	50	201	49	80,3

The output of the hybrid neural network matches the probabilities with the object in the database. The frame with the maximum probability is selected and accepted as the final output for the moment. The number of errors was 23-40%.

The recognition results in Table 3 were obtained from image processing.

Table 3. When test data that is unfamiliar to the system is trained by image processing.

№	Name of category	Total tests	Right	Incorrect	Percent
1	Cholesteatoma	45	227	18	92,9
2	Healthy ear	50	228	22	91,3

After morphological filtering, the results of Table 1 were obtained. 3. The number of errors was 8-9%.

Summary

Table 3 results were obtained after fuzzy image processing. The number of errors was 8-9%. The accuracy of calculations was increased by processing fuzzy images.

Conclusion

In conclusion, table 3 results were obtained after fuzzy image processing. The error rate was 8-9%. The accuracy of calculations was increased by processing fuzzy images. The use of non-parametric analysis algorithms showed better results and a much smaller amount of data compared to hybrid neural network algorithms. Regardless of the number of objects that appeared in the image, they were all recognized and classified. However, despite the results obtained, the recognition rate for some classes was low. Therefore, it is necessary to pay attention to the process of normalizing the input data for training and test images. The more elements in the workout, the higher the accuracy.

REFERENCES

1. Hashimoto-Ikehara M, Mishiro Y, Kitahara T, Sakagami M. The 10-year disease-free rate of attic cholesteatoma based on a new staging system.7:289–292. J Int Adv Otol (2011)
2. Kakehata S, Watanabe T, Ito T, Kubota T, Furukawa T. Extension of indications for transcanal endo scopic ear surgery using an ultrasonic bone curette for cholesteatomas. Otol Neurotol. 35(1):101–107. PMID: 24136323 (2014)
3. Takahashi M, Yamamoto Y, Kojima H. Transcanal endoscopic approach for pars flaccida cholestea toma using a 70-degree angled endoscope. Eur Arch Otorhinolaryngol. 278(4):1283–1288 PMID: 33439340 (2021)
4. Swartz JD HM. Inflammatory disease of the temporal bone. In: Som PM, Curtin HD, editors. Head and Neck Imaging. 5th ed. St. Louis: Mosby; 2011. pp. 1183–1229.
5. Lingam RK, Bassett P. A Meta-Analysis on the Diagnostic Performance of Non-Echoplanar Diffusion Weighted Imaging in Detecting Middle Ear Cholesteatoma: 10 Years On. Otol Neurotol. 38(4):521–528. PMID: 28195998 (2017)

6. Muzaffar J, Metcalfe C, Colley S, Coulson C. Diffusion-weighted magnetic resonance imaging for residual and recurrent cholesteatoma: a systematic review and meta-analysis. Clin Otolaryngol. 42 (3) :536–543. PMID: 27701821 (2017)
7. Baba A, Takahashi M, et al. Non-echoplanar diffusion weighed imaging and T1-weighted imaging for cholesteatoma mastoid extension. Auris Nasus Larynx. Oct; 48(5):846–851. PMID: 33461853. (2021)
8. OECD Indicators. Health at a Glance 2021. (2021)
9. Takahashi Y, Sone K, Noda K, Yoshida K, Toyohara Y, Kato K, et al. Automated system for diagnosing endometrial cancer by adopting deep-learning technology in hysteroscopy. PLoS One. 16(3): e0248526. PMID: 33788887. (2021)
10. Abdul-Aziz D, Kozin ED, Lin BM, Wong K, Shah PV, Remenschneider AK, et al. Temporal bone com puted tomography findings associated with feasibility of endoscopic ear surgery. Am J Otolaryngol. 38(6):698–703. PMID: 28711236 (2017)
11. Badran K, Ansari S, Al Sam R, Al Husami Y, Iyer A. Interpreting pre-operative mastoid computed tomography images: comparison between operating surgeon, radiologist and operative findings. J Laryngol Otol. 130(1):32–37. PMID: 26745138 (2016)